5294–5307 *Nucleic Acids Research, 2021, Vol. 49, No. 9* *Published online 20 April 2021*
doi: 10.1093/nar/gkab238

A ribonuclease III involved in virulence of Mucorales fungi has evolved to cut exclusively single-stranded RNA

José Tomás Cánovas-Márquez [1], Sebastian Falk [2,*], Francisco E. Nicolás [1], Subramanian Padmanabhan [3], Rubén Zapata-Pérez [4], Álvaro Sánchez-Ferrer [4], Eusebio Navarro [1,*] and Victoriano Garre [1,*]

[1]Department of Genetics and Microbiology (Associated Unit to IQFR-CSIC), Faculty of Biology, University of Murcia, 30100 Murcia, Spain, [2]Department of Structural and Computational Biology, Max Perutz Labs, A-1030 Vienna, Austria, [3]Instituto de Química Física "Rocasolano," Consejo Superior de Investigaciones Científicas, 28006 Madrid, Spain and [4]Department of Biochemistry and Molecular Biology-A, Faculty of Biology, Regional Campus of International Excellence "Campus Mare Nostrum," University of Murcia, Campus Espinardo, 30100, Murcia, Spain

Received July 22, 2020; Revised February 16, 2021; Editorial Decision March 22, 2021; Accepted March 24, 2021

ABSTRACT

Members of the ribonuclease III (RNase III) family regulate gene expression by processing double-stranded RNA (dsRNA). This family includes eukaryotic Dicer and Drosha enzymes that generate small dsRNAs in the RNA interference (RNAi) pathway. The fungus *Mucor lusitanicus*, which causes the deadly infection mucormycosis, has a complex RNAi system encompassing a non-canonical RNAi pathway (NCRIP) that regulates virulence by degrading specific mRNAs. In this pathway, Dicer function is replaced by R3B2, an atypical class I RNase III, and small single-stranded RNAs (ssRNAs) are produced instead of small dsRNA as Dicer-dependent RNAi pathways. Here, we show that R3B2 forms a homodimer that binds to ssRNA and dsRNA molecules, but exclusively cuts ssRNA, in contrast to all known RNase III. The dsRNA cleavage inability stems from its unusual RNase III domain (RIIID) because its replacement by a canonical RIIID allows dsRNA processing. A crystal structure of R3B2 RIIID resembles canonical RIIIDs, despite the low sequence conservation. However, the groove that accommodates dsRNA in canonical RNases III is narrower in the R3B2 homodimer, suggesting that this feature could be responsible for the cleavage specificity for ssRNA. Conservation of this activity in R3B2 proteins from other mucormycosis-causing Mucorales fungi indicates an early evolutionary acquisition.

GRAPHICAL ABSTRACT

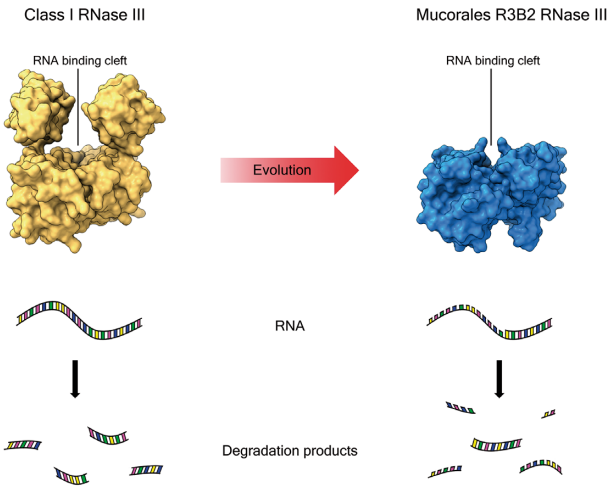

INTRODUCTION

RNA degradation is essential for gene regulation in all living organisms because it allows rapid adjustment of RNA abundance in response to environmental changes (1–4). Most of the endoribonucleases involved in regulation belong to the ribonuclease III (RNase III) family that is characterized by the ability to cleave specifically double-stranded RNA regions (dsRNA) (4). Loss-of-function mutations of RNases III induce global gene expression changes in bacteria and eukaryotes (5–7). This family includes the eukaryotic Drosha and Dicer enzymes of the RNA interference (RNAi) pathway that produce the microRNAs (miR-

*To whom correspondence should be addressed. Tel: +34 868887148; Email: vgarre@um.es
Correspondence may also be addressed to Eusebio Navarro. Tel: +34 868 889293; Email: sebi@um.es
Correspondence may also be addressed to Sebastian Falk. Tel: +43 1 4277 74360; Email: sebastian.falk@univie.ac.at

NAs) that control the gene expression of a large number of genes in plants and animals (8). Cleavage of dsRNA is performed by using two RNase III nuclease domains (RIIID) that are either in the same molecule, as in Dicer and Drosha (9,10), or in different molecules that form homodimers, as in bacterial and eukaryotic class I RNase III (11,12).

The fungus *Mucor lusitanicus,* formerly named *M. circinelloides* f. *lusitanicus,* is an outstanding model of early-diverging fungi because of its genetic tractability and the presence of several RNAi regulatory pathways (13). Moreover, *M. lusitanicus*, like other members of the Mucorales order, is an opportunistic human pathogen that causes the mucormycosis, a deadly infection with reduced treatment options (14,15). Unlike most fungi, mutants of *M. lusitanicus* in components of the RNAi machinery show clear defects in development, response to stress, and pathogenesis (13,16) resulting from changes in gene expression (17) mediated by mRNA-derived small RNAs (18,19). *Mucor lusitanicus* controls gene expression by three different RNAi-regulatory pathways, which are established through combinations of different RNAi components. Two of these RNAi pathways depend on Dicer and Argonaute proteins and are consequently considered as canonical (20). One of these canonical pathways, named epimutational, is important for pathogenesis because it produces transient drug resistant epimutants (21,22). The third pathway, described as non-canonical RNAi pathway (NCRIP), is independent of Dicer and Argonaute but requires RNA dependent RNA polymerases (RdRPs) and an endoribonuclease activity that has been attributed to R3B2, a protein that contains an atypical RIIID and two dsRNA binding domains (dsRBD) (19). NCRIP regulates the expression of specific genes by degrading their mRNAs. The degradation products show an undefined size, a very strong bias for uracil in the penultimate position, and most of them are sense to the mRNA, suggesting the participation of an endoribonuclease that cuts ssRNA (19). Transcriptomic analyses suggest that NCRIP regulates genes required to confront stressful environments such as phagocytosis by macrophages, being essential for virulence (16). Moreover, this pathway interacts with canonical RNAi pathways that either protect genome stability by controlling transposon mobilization or mediate the generation of epimutants (16,20).

Despite the relevance of NCRIP and its links with the canonical mechanisms, many functional aspects of this pathway remain unclear, including how specific mRNAs are targeted and then degraded to produce single-stranded small RNAs (19). The latter aspect is especially intriguing because R3B2 contains an atypical RIIID and thus far all RNases III have been described as specific for dsRNA (4,23). In this work, we provide evidence that R3B2 interacts with itself and thus forms homodimers as is observed for typical RNase III. However, it differs from them because it can bind both ssRNA and dsRNA through its dsRNA binding domains yet can only degrade ssRNA. In addition, we have determined the structure of the dimeric RIIID core and demonstrated that the unusual activity of R3B2 is conserved among the R3B2 family. These results support the proposed mode of action of the NCRIP and, more interestingly, represent the first example of an RNase III that has evolved to cut exclusively ssRNA.

MATERIALS AND METHODS

Strains, growth and transformation conditions

Mucor lusitanicus strain R7B (24), a leucine auxotroph derived from strain CBS277.49, and *Lichtheimia corymbifera* strain FSU9682 were used as the source of RNA for cDNA synthesis and cloning. *Saccharomyces cerevisiae* strains PJ69–4a and PJ69–4α (25) were used for yeast two-hybrid assays. *Escherichia coli* strain DH5α was used for all cloning experiments and strain BL21(DE3) (NEB, Cat. C2527) for the expression of recombinant protein.

Mucor lusitanicus and *Lichtheimia corymbifera* cultures were grown at 26 or 30°C, respectively in liquid minimal medium with Casamino Acids (MMC) (26) with pH 4.5 for 24 h, under illumination conditions and shaking (200 rpm).

Yeast cultures were grown at 30°C in YPAD complex medium or dropout Synthetic Defined (SD) medium without the appropriate amino acids for transformants selection. Solid media preparation was done by adding 20 g/l of agar. Yeast transformations were performed with 150–300 ng of bait or prey constructed vector, by PEG3350-lithium acetate method as described previously (27).

Unless indicated, bacterial cultures were grown at 37°C in lysogeny broth (LB) medium, supplemented with ampicillin (100 μg/ml) or chloramphenicol (50 μg/ml) when necessary. For solid media preparation, 15 g/l of agar was added.

RNA manipulation and analysis

Total RNA was isolated from 100 mg of *Mucor* or *L. corymbifera* mycelium using Trizol reagent (Invitrogen, Cat. 15596018), following the supplier recommendations. Expand Reverse transcriptase (Roche, Cat. 11785826001) and Herculase II fusion DNA polymerase (Agilent, Cat. 600675) were used in retrotranscription and PCR amplifications, respectively. Primer sequences are listed in Supplementary Table S1. Total RNA from R7B was reverse transcribed with Race-T primer and the desired cDNA was amplified with specific primers for each gene that included the required restriction sequences, cloned and sequenced to ensure the absence of mutations. Supplementary Table S2 describes the plasmids used in this work and their construction.

Secondary structures in single-stranded RNA was predicted using the Vienna RNAfold server (http://rna.tbi.univie.ac.at/cgi-bin/RNAWebSuite/RNAfold.cgi) (28)

Yeast two-hybrid assays

For characterization of the R3B2 self-interaction, *S. cerevisiae* pJ69–4a strain was transformed with both pBD-Gal4 (*Trp1*) and pACTII (*Leu2*) derived plasmids expressing *r3b2* or its fragments. Yeast transformations were plated on SD without tryptophan and leucine (SD-WL) and grown for 72 h at 30°C. Individual colonies from SD-WL plates were striped on SD without tryptophan, leucine, and histidine and supplemented with 2.5 mM of 3-amino-1,2,4-triazole (SD-WLH + 3AT) and SD without tryptophan, leucine and adenine (SD-WLA) to detect weak and strong interaction, respectively. A replicate was done on SD-WL as a transfer

control. The plates to assay the interaction were incubated for 2 weeks at 30°C.

Recombinant protein expression and purification

The pre-cultures were prepared by inoculating freshly transformed BL21(DE3) colonies in 30 ml of LB, supplemented with ampicillin. Expression plasmids used for this purpose are described in Supplementary Table S2. Overnight grown cultures (at 37°C and 250 rpm) were diluted in fresh media (1:25) and incubated in the same conditions until achieving an OD_{600} of 0.6–0.8. At this point, the expression of recombinant proteins was induced by adding 1 mM of isopropyl β-D-1-thiogalactopyranoside (IPTG) to the culture and incubating for overnight (at 26°C and 250 rpm). After induction, the cultures were cooled down on ice and centrifuged at 3000 × *g* for 15 min at 4°C. The supernatant was discarded, and the cell pellet was stored at -80°C.

For the recombinant protein purification under non-denaturing conditions, cell pellets from 100 ml culture were thawed on ice for 15 min and resuspended in 5 ml of Start buffer (STB) (50 mM NaH_2PO_4; 300 mM NaCl; 1 mM dithiothreitol; pH 8.0), with 5 μl of each 1 M benzamidine and 1 M phenylmethylsulfonyl fluoride (PMSF). The cell suspension was sonicated, and the lysate was centrifuged at 10 000 × *g* for 30 min at 4°C to obtain a cleared cell lysate that was transferred to a new tube. About 1 ml of Ni-NTA Agarose beads (50% slurry) (Qiagen, Cat. 30210) were equilibrated in STB and added to the cleared lysate. The mix was incubated for 1 h at 4°C in a rotatory shaker to allow the binding of 6× His-Tagged proteins. After incubation, the beads were centrifuged at 2000 rpm for 5 min at 4°C and the supernatant discarded. To reduce the nonspecific binding of proteins, the beads were washed three times with 10 ml of STB and twice with 10 ml of STB with 5% of Elution buffer (EB) (50 mM NaH_2PO_4; 300 mM NaCl; 1 mM DTT; 250 mM Imidazole, pH 8.0). Elution of 6× His-tagged proteins was carried out by resuspending the beads in 1 ml of STB with 20% serial increments of EB, and centrifugations at 6000 rpm for 1 min at 4°C. Each elution was recollected and stored at -80°C or directly analyzed in a 10% SDS-PAGE gel to select those containing the 6× His-Tagged protein. Buffer was exchanged by dialysis in 20 mM Tris-HCl, pH 8.0, 1 mM dithiothreitol, 1 mM EDTA and 10% glycerol. Protein samples were quantified with Bradford protein assay (Bio-Rad) following the supplier specifications.

Limited proteolysis analysis and characterization of the products

Purified R3B2 protein (50 μg) in 550 μl reaction buffer (100 mM NaCl, 50 mM Tris pH 7.5, 1 mM β-mercaptoethanol) was digested with subtilisin Carlsberg (Sigma-Aldrich) at 30°C (1:125 w/w protease:protein). Aliquots of 15 μl were removed from the reaction mixture and inactivated by adding 1 μl of 1 M benzamidine at 0, 15, 30, 45, 60, 75, 90 and 105 min. Then, 7.5 μl of 4× NuPAGE LDS sample buffer (Novex) and 2 μl of β-mercaptoethanol were added to each sample and analyzed in 15% SDS-PAGE gels. Gels were stained with Coomassie Blue.

The molecular weights of subtilisin resistant fragments were determined, at the Molecular Biology facility of the University of Murcia (ACTI), by mass spectrometry (ESI-Ion trap) of a 30-min subtilisin-digested sample filtered with a 0.22 μm filter using an Agilent 6100 Series TOF Mass Spectrometer (Agilent Technologies, Santa Clara, CA, USA) with an electrospray (ESI) interface. For N-terminal sequencing (NTS), the 30-min digested sample was subjected to electrophoresis in a NuPAGE 12% Bis-Tris gel (Novex) and the subtilisin-resistant bands were electrotransferred to an Immobilon PSQ membrane (Millipore) following the supplier recommendations. After staining with Coomassie Blue, the bands were excised to be subject to NTS at the Margarita Salas Center for Biological Research (CIB-CSIC) facilities. For peptide mass fingerprinting, the 15-, 30- and 105-min samples were subjected to electrophoresis in a NuPAGE 12% Bis-Tris gel. Subtilisin-resistant bands were identified by Coomassie Blue staining and each excised from the most concentrated sample was analyzed by peptide mass fingerprinting using 6× His-R3B2 sequence as query. Each fragment NTS read and fingerprint-resulting peptides were associated with their corresponding molecular weight to define their complete amino acid sequence.

Protein crystallization and structure determination

A fragment containing residues 1–273 of R3B2 was cloned into a modified pET-vector with a 6xHis-Thioredoxin (Trx) tag followed by a 3C protease cleavage site. R3B2 was purified similarly as described above. The His-Trx tag was cleaved with His-tagged 3C protease and both the His-Trx tag and 3C protease were removed using Ni-NTA agarose beads. R3B2 was concentrated using ultrafiltration and subjected to size-exclusion chromatography on a Superdex 200 (16/600) column equilibrated in 20 mM Tris/HCl pH 7.5, 150 mM NaCl, 5 mM $MgCl_2$ and 2mM dithiothreitol. After size-exclusion chromatography, R3B2 was concentrated to 14 mg ml^{-1} and stored at -80°C until further use. Crystallization trials were performed using a vapor diffusion set-up by mixing the protein complex and crystallization solution in a 2:1 ratio. Initial crystals grew in 50 mM Mes/NaOH pH 6.0, 4% MPD, 200 mM ammonium acetate and 30% (w/v) PEG3350 at 18°C. The initial hit was refined to 100 mM Hepes/NaOH pH 7.0, 200 mM L-proline and 12% (w/v) PEG3350. The crystals were cryoprotected with the reservoir solution supplemented with 25% (v/v) glycerol before data collection at 100 K. All diffraction data were collected at the Swiss Light Source PXII beamline (Villigen, Switzerland). Data were processed with Xia2/Dials (29) within CCP4i2 (30). The crystals belong to the orthorhombic space group $P2_12_12_1$ and diffracted to 1.65 Å resolution. For phasing, the crystals were soaked for 2 min with reservoir solution supplemented with 0.4 M NaI and 25% (v/v) glycerol. The structure of R3B2 was solved by single isomorphous replacement with anomalous scattering (SIRAS) phasing with Autosol from Phenix (31). The mean figure of merit over all resolution shells had a value of 0.35 and estimated map correlation coefficient a value of 51.3 ± 17.6. Most of the model was automatically built using Autobuild, and was manually completed with COOT (32) and refined with refmac5 (33) and phenix (34). Data collection, phasing and refinement statistics are listed in Supplementary Table

S3. Molecular graphics of the R3B2 structure were created using UCSF ChimeraX (35).

Size-exclusion chromatography coupled to multi-angle light scattering (SEC MALS)

The molecular mass and the oligomeric state of R3B2 1–273 in solution were determined by size exclusion chromatography (SEC) coupled to multi-angle light scattering (MALS). A Superdex 200 Increase 10/300 GL column (GE Healthcare Life Sciences) was connected to a 1260 Infinity HPLC system (Agilent Technologies) coupled to a MiniDawn Treos detector (Wyatt Technologies) with a laser emitting at 690 nm. An RI-101 detector (Shodex) was used for refractive index measurement. Data analysis was performed using Astra 7 software package (Wyatt Technologies).

Electrophoretic mobility shift assays

Radiolabeled RNAs were transcribed from PCR templates amplified from genes *carB* (ID 31317), *P1* (ID 155412) or *mcwc-1b* (ID 149173) by T7 RNA polymerase (Thermo Scientific, Cat. EP0111) with [α-^{32}P]UTP following the supplier recommendations. Primers used for the template amplification are listed in Supplementary Table S1. GAstair ssRNA was transcribed from pMAT2304 linearized with EcoRV (Supplementary Table S2). For dsRNA synthesis, sense and antisense templates were transcribed together in the same reaction. Free nucleotides were removed by Sephadex G-50 Fine column. dsRNA preparations were treated with 4 μl of RNase A/T1 mix (Thermo scientific, Cat. EN0551) in 150 μl of 10 mM Tris-HCl pH 7.5, 300 mM NaCl and 5 mM EDTA for 30 min at 37°C for ssRNA removing. Both ssRNA and dsRNA preparations were subjected to Trizol reagent (Invitrogen, Cat. 15596018) extraction following the supplier recommendations and resuspended in Molecular biology grade H_2O. Binding reactions (10 μl) were performed by incubating the radiolabeled ssRNA or dsRNA with the proteins at the indicated concentrations in 30 mM Tris-HCl pH 7.4, 30 mM NaCl, 5 mM $MgCl_2$, 1 mM dithiothreitol and 0.1 mM EDTA. For reactions with GAstair ssRNA, 0.01 mg/ml of BSA was added to avoid RNA precipitation. Reactions were incubated at room temperature for 30 min and fractionated by 4% PAGE (37.5%:1% (w/v) acrylamide/bis-acrylamide) in 0.5× TBE buffer at 200 V for 60 min. After electrophoresis, RNA was visualized by autoradiography.

In vitro RNase activity assays

Radiolabeled RNA substrates and RNase reactions were prepared as described for EMSA. PCR templates were obtained from plasmid pMAT688 for ssRNA transcription and plasmids pMAT679 and pMAT688 for dsRNA, using primers pairs STU/pMAT679-Rev1 and STU/pMAT688-Rev1, respectively. Primer sequences used for the template amplification are listed in Supplementary Table S1. Reactions were incubated at 30°C overnight and fractioned by 16% PAGE (19%:1% (w/v) acrylamide/bis-acrylamide) containing 7 M urea in 0.5× TBE buffer at 300 V for 1.5 to 2 h. After electrophoresis, RNA was visualized by autoradiography.

Phylogenetic analysis of R3B2 family amino acid sequences

R3B2 protein from *M. lusitanicus,* as well as the other RNase III-like protein, an MRPL3 homolog (ID 110239), were used as queries in a BLAST search of homologs of R3B2 in Mucoromycota genomes. Species names and JGI accession numbers of all sequences used are indicated in the phylogenetic tree. Bacterial RNase III protein RNC from *E. coli* (P0A7Y0) and *Aquifex aeolicus* (O67082), and the nuclear RNase III proteins from *S. cerevisiae* (Q02555), *Schizosaccharomyces pombe* (P22192), *Neurospora crassa* (V5IQ18), *Aspergillus niger* (G3XLX0), *C. neoformans* (Q5KEY8) and *C. albicans* (A0A1D8PM79; A0A1D8PM62), were also included in the phylogenetic analysis. Representative homologs from each Mucoromycota group were aligned by MUSCLE v3.8.31 (36) and truncated proteins without a RIIID or dsRBD were discarded by manual curation prior to the analysis. The phylogenetic tree was inferred by PhyML v3.0 (37), using the best model with 1000 bootstrap replicates.

RESULTS

Characterization of structured domains in R3B2 protein

Classical class I RNase III proteins adopt a homodimeric architecture, mediated by the RIIID, that allows the cleavage of each strand in dsRNA (11,38). Interaction of R3B2 with itself in a yeast two-hybrid (Y2H) system (Figure 1A) suggested that it is a class I RNase III. To identify both structural domains within R3B2 and the regions involved in self-interaction, we subjected R3B2 to limited proteolysis. Unstructured or partially structured regions of proteins are more accessible and, therefore, more susceptible toward proteases than compact structured domains (39). R3B2 was expressed in *E. coli* and the purified protein was incubated with subtilisin, a broad specificity protease. Aliquots were taken at different time points to visualize the digestion products in SDS-PAGE (Figure 1B). The most abundant fragments were named according to their apparent molecular weight in kDa as F22, F19, F18 and F14 (F for fragment) (Figure 1C). F18 and, to a lesser extent F14 were the most resistant fragments to the protease treatment. Next, we determined the molecular weights of the subtilisin resistant fragments by mass spectrometry and their sequence by N-terminal sequencing and peptide mass fingerprinting using a 30-min technical replicate (Figure 1D). The results suggested that F22 and F19 were degradation products that finally yielded F18, which contains a well-structured atypical RIIID, while F14 was derived from the dsRBD proximal to the RIIID. In contrast, no stable fragment corresponding to the C-terminal region of the protein that includes a second predicted dsRBD was detected, suggesting that this part of R3B2 is less structured.

The presence of two well-structured domains in the protein prompted us to further analyze the previously detected self-interaction of R3B2. Therefore, gene fragments encoding F18, F14, and the C-terminal region of R3B2 (CTF), which covers the rest of the protein, were cloned in yeast

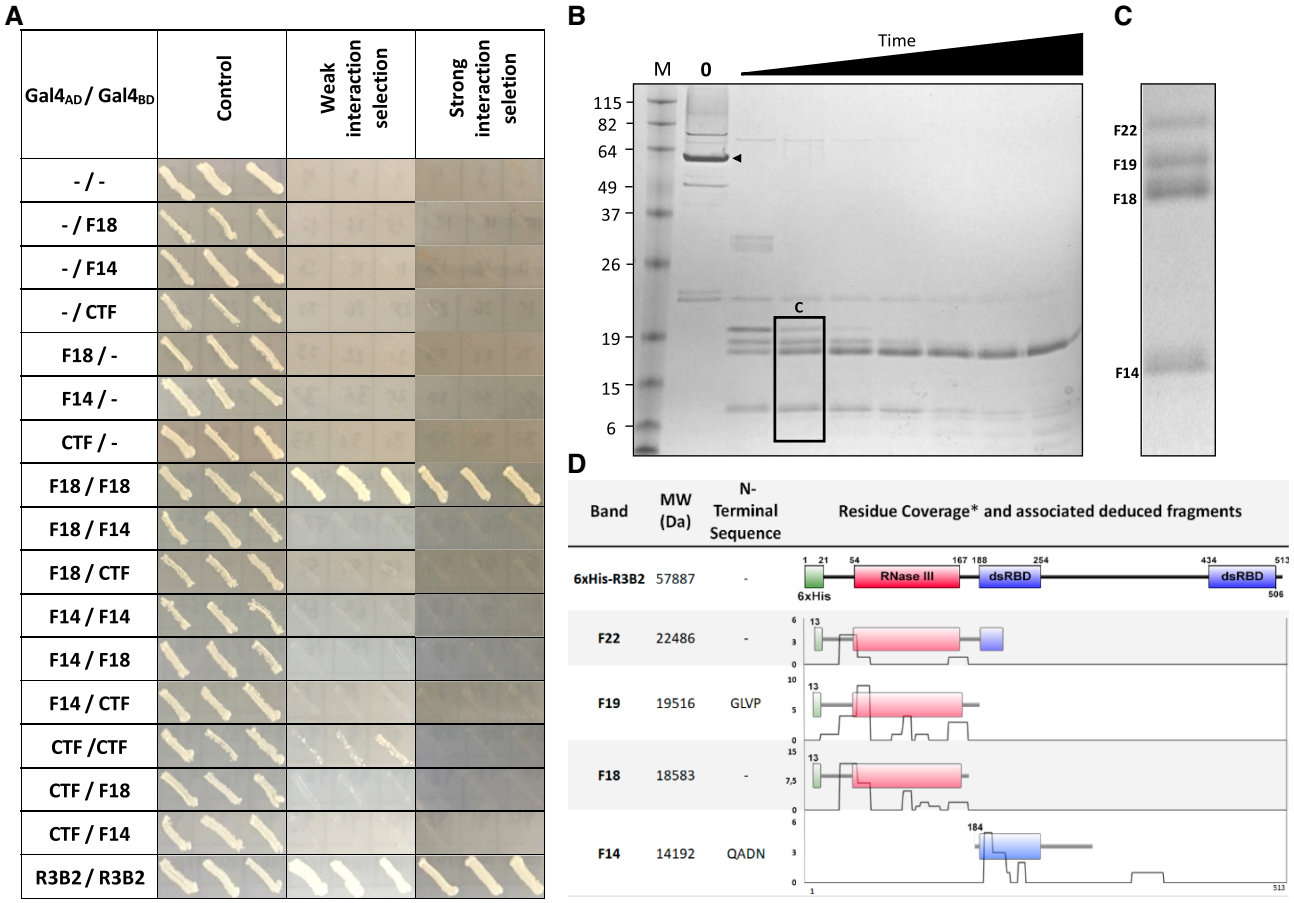

Figure 1. Characterization of structured domains in R3B2 protein. (**A**) The interaction of F18, F14, and CTF containing the RIIID, the first dsRBD, and the C-terminal region of the R3B2 harboring the second dsRBD, respectively, was analyzed in comparison to the full-length R3B2 protein by growing the yeast colonies for 3 days in selective medium for weak and strong interaction. -, Empty Gal4 AD or BD. (**B**) Purified R3B2 protein (Lane 0) was treated with subtilisin for 15, 30, 45, 60, 75, 90 and 105-min. M, BenchMark Pre-stained Protein ladder (Invitrogen). (**C**) Detail of R3B2 derived fragments after 30 min of digestion. (**D**) Identification of R3B2 derived fragments according to their characteristics. *Sequences obtained from peptide mass fingerprint were aligned with the protein and represented as residue coverage.

vectors to express both Gal4 AD and Gal4 BD fusion proteins. Y2H assays analyzing all possible interactions among these fragments revealed a strong interaction of F18 with itself, and also a weak interaction of CTF with itself (Figure 1A). Furthermore, size exclusion chromatography and static light scattering of a protein fragment that included the stable fragments F18 and F14 (ΔCTF) supported the homodimerization of R3B2 (Supplementary Figure S1). These results are consistent with considering R3B2 as a member of the RNase III protein family because inter or intramolecular dimerization of the catalytic domains is a pervasive feature of this family (40).

Binding of RNAs by R3B2 relies on both dsRBDs

The hypothesis that R3B2 is the enzyme involved in the degradation of specific mRNAs in the NCRIP requires that the protein can bind RNA. The ability of R3B2 to interact with RNA molecules and the role of the dsRBDs in the binding was analyzed *in vitro* by electrophoretic mobility shift assay (EMSA). Full-length R3B2 expressed and purified from *E. coli* was incubated with ^{32}P-labeled ssRNA or dsRNA and then the RNA–protein complexes resolved by native PAGE. The results revealed that R3B2 was able to bind both a 103-nt ssRNA and 100-bp dsRNA (Figure 2A, B) corresponding to the *carB* gene.

Increasing the R3B2 concentrations resulted in two differentially migrating species with intermediate and low mobility. At high R3B2 concentrations, the species of intermediate mobility was converted to the low mobility species, suggesting binding of multiple R3B2 dimers. The complete shift of RNA fragments was observed when the protein dimer/RNA ratio was higher than two (Figure 2A, B), suggesting that this higher band is the result of the binding of two R3B2 dimers to the RNA molecule.

Considering that 103-nt ssRNA substrate might contain regions prone to form double-stranded regions, e.g. hairpins, we designed a synthetic fragment of the same length consisting of tandem GA repeats, with five interspersed Us for labelling, to avoid formation of dsRNA (according to the Vienna RNAfold server (28)). This ssRNA substrate, named GAstair, was bound by R3B2 producing a similar shift mobility pattern as the *carB* ssRNA and dsRNA (Supplementary Figure S2A), confirming that R3B2 can bind

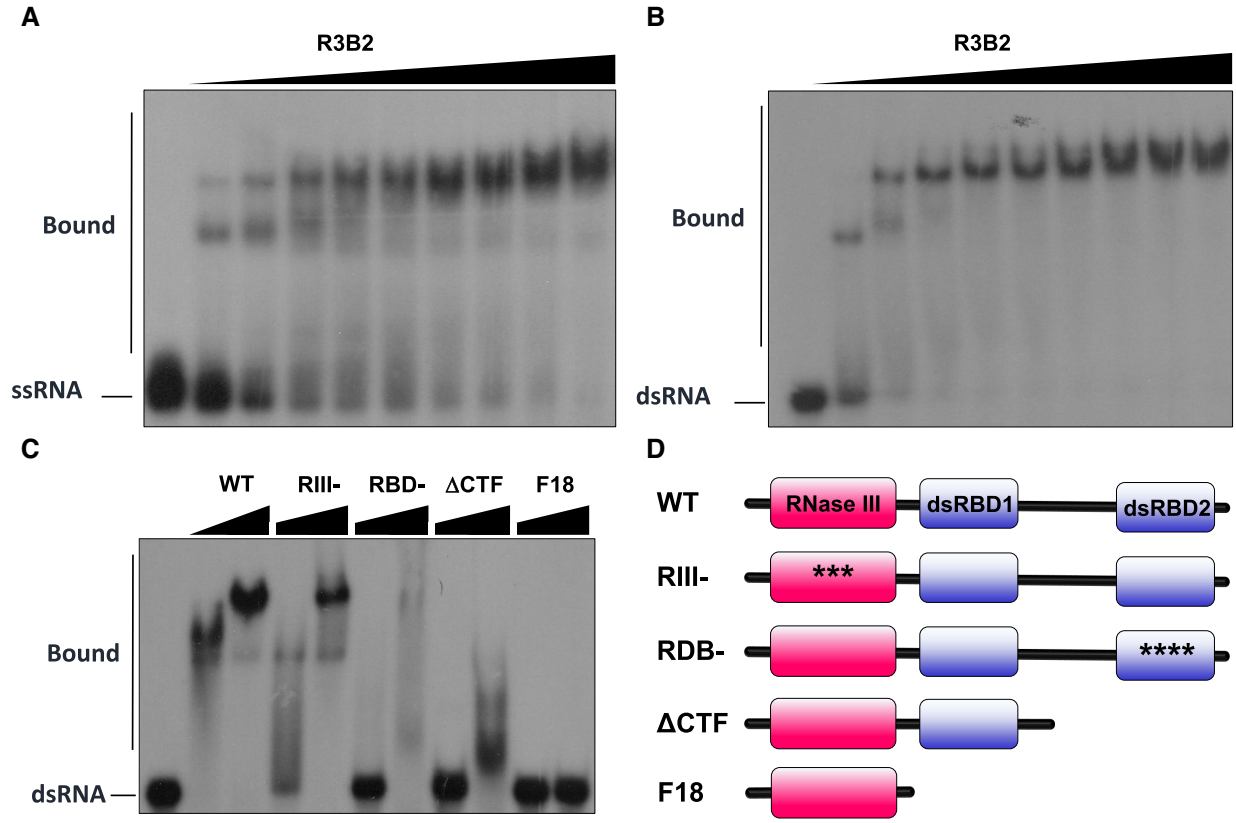

Figure 2. Characterization of RNA binding by R3B2 and influence of dsRBDs. (**A**) EMSA of R3B2 against 103-nt ssRNA (100 nM *carB100* ssRNA; protein concentration: 50, 100, 150, 200, 250, 300, 350, 400 and 450 nM). (**B**) EMSA of R3B2 against 100-bp dsRNA (50 nM carB100 dsRNA; protein concentration: 50, 100, 150, 200, 250, 300, 350, 400 and 450 nM). (**C**) EMSA of R3B2 and mutant or truncated versions against 100-bp dsRNA (60 nM *carB100* dsRNA; protein concentration for each: 200 and 500 nM). (**D**) Schematic representation of R3B2 and mutated or truncated versions used in EMSA.

ssRNA *in vitro*. This binding *in vitro* was independent of the RNA sequence as the EMSA with different RNAs, including mRNA fragments from genes that are regulated or not by the RNAi-related pathways of *M. lusitanicus*, gave similar results (Supplementary Figure S2). The binding of R3B2 to both ssRNA and dsRNA molecules support the hypothesis that R3B2 binds mRNA containing short double stranded stretches generated by the action of the RdRPs (19).

To identify the structural R3B2 elements required for the RNA binding, we tested the binding ability of protein versions with point mutations in key residues or deletion of the dsRBDs (Figure 2C, D). All mutant versions of R3B2 were expressed in *E. coli* and purified using a His-tag. Previous results had shown that an *r3b2* mutant allele coding for a protein, named R3B2(RIII-), in which three conserved amino acids of the RNase III family signature (Prosite PS00517) were replaced by alanines (H49A, G55A, E56A) was unable to complement the *r3b2* deletion *in vivo* (19). In EMSA assays, this protein showed a slight reduction in RNA binding (Figure 2C, lane RIII-), indicated by the presence of complex bands smeared at low concentration of protein that suggested that the complexes may be destabilized during the electrophoresis (41). Conversely, RNA binding of mutant proteins lacking dsRBD2 was severely affected because no stable complex formation was observed even at high protein concentration (Figure 2C, lane ΔCTF). A similar defect in the interaction with dsRNA was observed when a cluster of five basic residues (R469A, R470A, K471A, K472A) corresponding to the conserved region 3 of dsRBD2, probably involved in the recognition of dsRNA major groove (42), was replaced by alanines (Figure 2C, lane RBD-). Deletion of both dsRBDs provoked a drastic loss of the affinity of R3B2 for RNA, indicating that both dsRBDs are necessary for efficient binding to RNA (Figure 2C, lane F18).

R3B2 cuts only ssRNA

Since NCRIP produces mainly sense sRNAs derived from the target mRNAs, it was proposed that the ribonuclease involved in this pathway, likely R3B2, should cut only ssRNAs (19). However, R3B2 harbors an atypical RIIID, which suggested that R3B2 might cut dsRNA instead of ssRNA. Therefore, we tested the activity of R3B2 toward both ssRNA and dsRNA substrates.

Incubation *in vitro* synthesized ^{32}P-labeled ssRNA or dsRNA molecules with the full-length R3B2 and subsequent PAGE showed that the ssRNA was degraded producing a smear along the whole lane (Figure 3A), whereas the dsRNA was not affected by the incubation with R3B2 (Figure 3B). The presence of a smear along the whole lane suggested that the cleavage of the ssRNA by R3B2 produced fragments of different lengths similar to that observed *in*

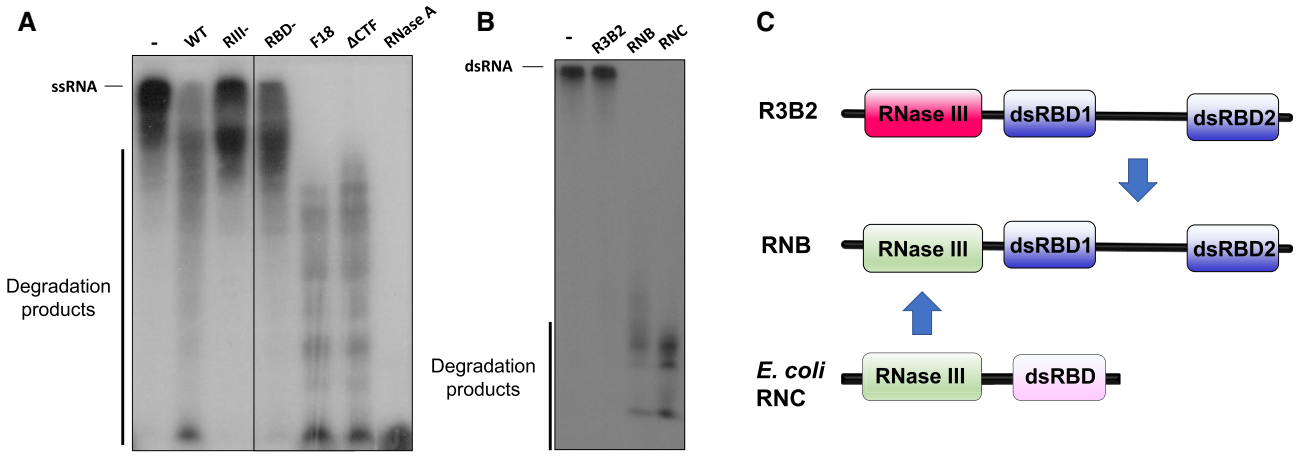

Figure 3. RNase activity of R3B2. (**A**) ssRNA (30 nM *carB* ssRNA) was treated with wild-type R3B2 or the mutant forms described in Figure 2 and resolved by PAGE (protein concentration: 150 nM). (**B**) dsRNA (30 nM *carB* dsRNA) was treated with R3B2, the chimeric protein RNB and RNC from *E. coli* and resolved by PAGE (protein concentration: 150 nM). (**C**) Schematic representation of R3B2, chimeric protein RNB and *E. coli* RNC protein.

vivo for the degradation of mRNAs by the NCRIP (19). The ability of R3B2 to cleave ssRNA was further supported by the GAstair substrate, as the addition of R3B2 also resulted in the generation of degradation products (Supplementary Figure S3). Interestingly, the degradation of ssRNA seen with the wild-type protein was not observed when mutant R3B2(RIII-) was used, indicating that the atypical RIIID is responsible for the catalytic activity of the protein. Similarly, the R3B2 protein with point mutations in the dsRBD2 (RBD-) was unable to degrade ssRNA, indicating that this RNA binding domain is essential for the cleavage. However, deletion of dsRBD2 (ΔCTF) or both dsRBDs (F18) enhanced the activity of R3B2 against ssRNA *in vitro* (Figure 3A), suggesting that the dsRBDs may modulate the R3B2 cleavage activity. Similarly, the *E. coli* RNase III (RNC) lacking the dsRBD can accurately cleave small processing substrates *in vitro* (43) as can class IV RNases III proteins (Mini-III) only containing a RIIID (44). As for other RNase III proteins (45–47), the R3B2 RNase activity was dependent on Mg^{2+} and was inhibited at high concentrations of this divalent cation (Supplementary Figure S4). These results indicated that R3B2 is an unusual RNase III that is able to cut ssRNA, but not dsRNA like other known RNase III proteins (4,23), and it is the RNase responsible for the degradation of specific mRNAs in the NCRIP.

The above results suggested that the inability of R3B2 to cut dsRNA depends on the atypical RIIID. To test this hypothesis, we generated a chimeric R3B2 protein, named RNB, in which its atypical RIIID was replaced by the canonical RIIID of RNC from *E. coli* (Figure 3C). RNase activity assays revealed that RNB was able to degrade dsRNA as did RNC and in contrast to R3B2 (Figure 3B). These results suggested that the loss of R3B2 ability to cleave dsRNA is fully determined by changes present in the catalytic domain of the protein.

Crystal structure of R3B2 RNase III-like domain

In order to understand how R3B2 differs from other RNase III enzymes, we purified and crystallized a fragment of R3B2 containing the RIII domain and the first dsRBD. Native crystals diffracted to 1.65 Å, but the structure could not be solved by molecular replacement. Therefore, we solved the structure experimentally by SIRAS using sodium iodide-soaked crystals. Crystallographic statistics are given in Supplementary Table S3. The R3B2 catalytic domain is well-ordered, however, density corresponding to dsRBD1 could not be observed, probably due to flexibility of the dsRBD1 in the absence of RNA substrate. We compared the R3B2 structure to those of the structurally best characterized RNase III proteins (*Aa*RIII (48), *Sc*RNT1 (49), *Hs*Drosha (50) and *Gi*Dicer (51)). Superposition with structures of *Aa*RIII and *Sc*RNT1 revealed an overall RMSDs of 2.4 and 2.2 Å, respectively (Figure 4A). The largest differences are found in the linkers connecting helices α2/α3 and α5/α6 (Figure 4A and Supplementary Figure S5A). The RNase III family contains two dsRNA-binding motifs (RBM) in the catalytic core domain, also known as RBM3 and RBM4 (38). Amino acid side-chains from RBM3 and RBM4 interact with the phosphoribose backbone of the RNA and thereby contribute to RNA binding. The structure-based sequence alignment revealed that RBM3 is present in R3B2, but the conserved glutamate in RBM3 corresponds to an asparagine (N76) in R3B2 (Figure 4B). RBM4 resides in the linker that connects helix α5 to α6, and is one of the regions that differs significantly between R3B2 and other RNase III family members. RBM4 varies from 11 residues in *Aa*RIII to 21 residues in *Sc*RNT1, but is only about three residues long in R3B2. Sequence analysis showed that RBM4 is absent throughout Mucorales and the only conserved residues in this region of R3B2 are L102 and V106, which are responsible for forming a tight turn connecting helices α5 and α6 (Supplementary Figure S5B).

Despite the cluster of acidic residues comprising E40, D44, D107 and E110 in the RNase III catalytic center of *A. aeolicus* not being absolutely conserved in R3B2 (Figure 4B), our crystallographic data for *M. lusitanicus* R3B2 revealed an architecture involving three acidic residues E56, E113 and D116 but with asparagine (N52) instead of an aspartate. Although the position of the acidic residues is conserved, the identities of Glu and Asp are inverted in comparison with *A. aeolicus* and other RNase III catalytic centers

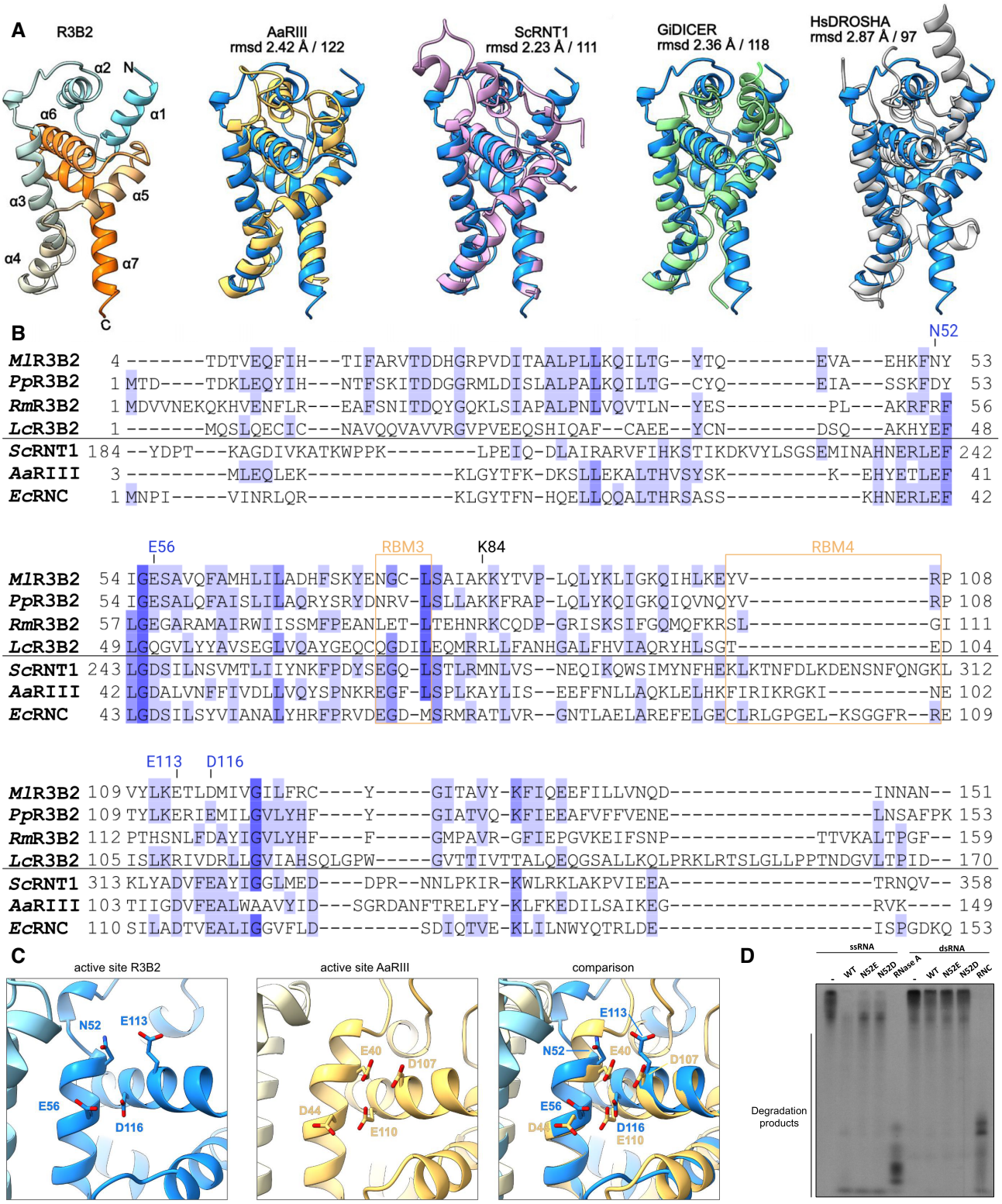

Figure 4. Structural analysis of R3B2 RNase III-like domain. (**A**) Comparison between RIII core domain of R3B2 to other RNase III proteins. On the left R3B2 is colored from blue to white to red from N to C-terminus and the helices are named. On the right, R3B2 is shown in blue and superimposed with different RIII proteins. The rmsd and the number of aligned residues are indicated. (PDC codes: AaIII: 2NUG; ScRNT1: 5T16; GiDICER: 2FFL; HsDROSHA: 6V5B. (**B**) Multiple sequence alignment of the RNase III-like core in *M. lusitanicus* R3B2 (*Ml*R3B2), *P. parasitica* (*Pp*R3B2), *R. microsporus* (*Rm*R3B2) and *L. corymbifera* (*Lc*R3B2) and comparison with bacterial (RNase III from *A. aeolicus* and RNC from *E. coli*) and fungal (Rnt1 from *S. cerevisiae*) RIIID. (**C**) Zoom-in views of the active sites of R3B2 (blue) and *Aa*RIII (yellow). Residues important for activity are shown as sticks. (**D**) RNase activity assay performed as described in Figure 3 using wild-type R3B2 and the mutants in the catalytic center of the protein (20 nM *carB* ssRNA; 10 nM carB dsRNA; protein concentration: 150 nM). -, untreated.

(38,49), but their relative arrangement is maintained except for N52 (Figure 4C). Therefore, we considered the possibility that the presence of N52 might weaken magnesium coordination required for efficient cleavage described elsewhere (12,38,49). To test this possibility, we constructed N52E and N52D versions of R3B2, and incubated them with labeled RNAs (Figure 4D). The results showed that both mutant versions were still able to cut ssRNA similar to the wild-type R3B2, but no cleavage activity against dsRNA, indicating that presence of asparagine in position 52 is not responsible for ssRNA cleavage activity.

The observation that R3B2 can bind both ssRNA and dsRNA but only cleaves ssRNA prompted us to compare structures of RNase III proteins bound to dsRNA. Superposition of R3B2 to *Aa*RIII and *Sc*RNT revealed the two protomers in R3B2 form a 'narrower' cleft compared than in *Aa*RIII and *Sc*RNT (Figure 5A). As the catalytic core of *Aa*RIII adopts an almost identical conformation in the presence and absence of dsRNA (Supplementary Figure S6), the 'narrow' conformation in R3B2 is most likely not caused by the absence of RNA. To model the dsRNA onto the R3B2 structure, we superposed one protomer of R3B2 to one protomer of *Aa*RIII and *Sc*RNT1. In this R3B2-dsRNA model, the RNA clashes severely with the R3B2 catalytic core. Most prominently, two lysine residues in R3B2 (K84) protrude from the RNA binding surface (Figure 5A). The presence of a positively charged amino acid (lysine or arginine) at this position is conserved in R3B2 proteins from other Mucorales (Figure 4B). To test if K84 was responsible of the substrate preference of the RNase, we generated protein versions in which this lysine was replaced by a small polar alanine (K84A), a negatively charged glutamate (K84E), and by glutamine (K84Q), with a side chain of similar length but uncharged and polar. All three R3B2 mutants behaved similarly to wild-type R3B2, they retained both the activity against ssRNA and the inability to cleave dsRNA (Figure 5B), suggesting that R3B2 either binds RNA differently compared to *Aa*RIII and *Sc*RNT1 or that RNA-binding induces conformational changes in the catalytic core of R3B2.

R3B2 activity is conserved in Mucorales

Previous studies determined that R3B2 family is restricted to the order Mucorales with members that contain one RIIID and either one or two dsRBDs (19). Due to the growing number of genome sequences, we explored in the Mucoromycota phylum for the presence of proteins similar to R3B2 and MRPL3, another RIIID containing protein. The protein search on all the eighty-six species from Mucoromycota phylum present in Mycocosm resources (https://mycocosm.jgi.doe.gov/) (52) found 71 and 88 proteins (expected value lower than 10^{-3}) similar to R3B2 and MRPL3, respectively. Duplicate proteins from different isolates of the same species and truncated hits lacking the RIIID or dsRBDs were removed, resulting in 36 proteins similar to R3B2. No other RNase III proteins were identified when using less stringent conditions. As expected, R3B2 proteins were restricted to the order Mucorales, while MRPL3 was present in all of studied species, but only 31 MRPL3 homologs representing the Mucoromycota diversity were selected for further analyses. The proteins were aligned together with other RNases III with similar domain architecture such as class I RNases III from bacteria and nuclear class II RNases III from fungi. The phylogenetic tree using the bacterial proteins as an outgroup clustered all R3B2 family members with a high bootstrap support (997/1000) and clearly separated from MRPL3 homologs and other fungal class II RNase III proteins (Figure 6A).

R3B2 family includes RNase III-like proteins with one or two dsRBDs with a great number of uncommon substitutions affecting catalytic amino acid residues of the RIIID harbored by canonical prokaryotic and eukaryotic proteins (Figure 4B). Surprisingly, residues in these positions in R3B2 showed low conservation in similar proteins of other Mucorales species. Therefore, we wondered if other members of the R3B2 family harbor RNase activity specific for ssRNA. Proteins from three species covering the Mucorales phylogeny were selected for their expression in *E. coli* and analysis of their RNase activity. The selected proteins were from the mycoparasite *Parasitella parasitica* (*Pp*R3B2) and from the mucormycosis causing agents *Rhizopus microsporus* (*Rm*R3B2) and *L. corymbifera* (*Lc*R3B2). All of them contained only one dsRBD and *Lc*R3B2 showed a very low conservation of the catalytic amino acid residues (Figure 4B). As with *M. lusitanicus* R3B2 (*Ml*R3B2), also *Pp*R3B2, *Rm*R3B2 and *Lc*R3B2 degraded ssRNA, but not dsRNA (Figure 6B), suggesting that all three are true orthologs of *Ml*R3B2 that have lost the ability to cleave dsRNA but conserved the cleavage activity toward ssRNA, despite their sequence differences in the RIIID.

DISCUSSION

Mucormycosis is a devastating infection considered emergent because of its growing incidence in recent years (53). The natural resistance to antifungals of the causative species and the reduced knowledge about the Mucorales biology result in a small number of therapeutic options (54). NCRIP has an important role in pathogenesis as it regulates the fungal response to phagocytosis by macrophages (16). Moreover, NCRIP represents an opportunity to investigate the evolution of the RNAi because it functions as a degradation pathway of specific mRNAs with the participation of RNA dependent RNA polymerases (RdRP) (19,20), which are typical RNAi enzymes (55). The involvement of RNAi proteins in this pathway suggested NCRIP could represent the first step in the evolution of the RNAi mechanism (19). According to this proposal, Dicer and Argonaute do not participate in NCRIP and R3B2 is the only hypothetical endoribonuclease demonstrated to participate in this mechanism *in vivo* (19). The domain organization of R3B2 with one RIIID and two dsRBDs is similar to class I RNases III, which are broadly distributed in bacteria, but also found in diverse eukaryotes and some viruses (56). Despite the similarity to class I RNases III, R3B2's atypical RIIID lacks critical amino acids of the RNase III family signature (Prosite PS00517) to be considered as a true RNase III and NCRIP degradation products are ssRNAs without defined size, as opposed to size-specific dsRNA products produced by Dicer in canonical RNAi (19). Our hypothesis that R3B2 could bind to dsRNA regions in mRNAs

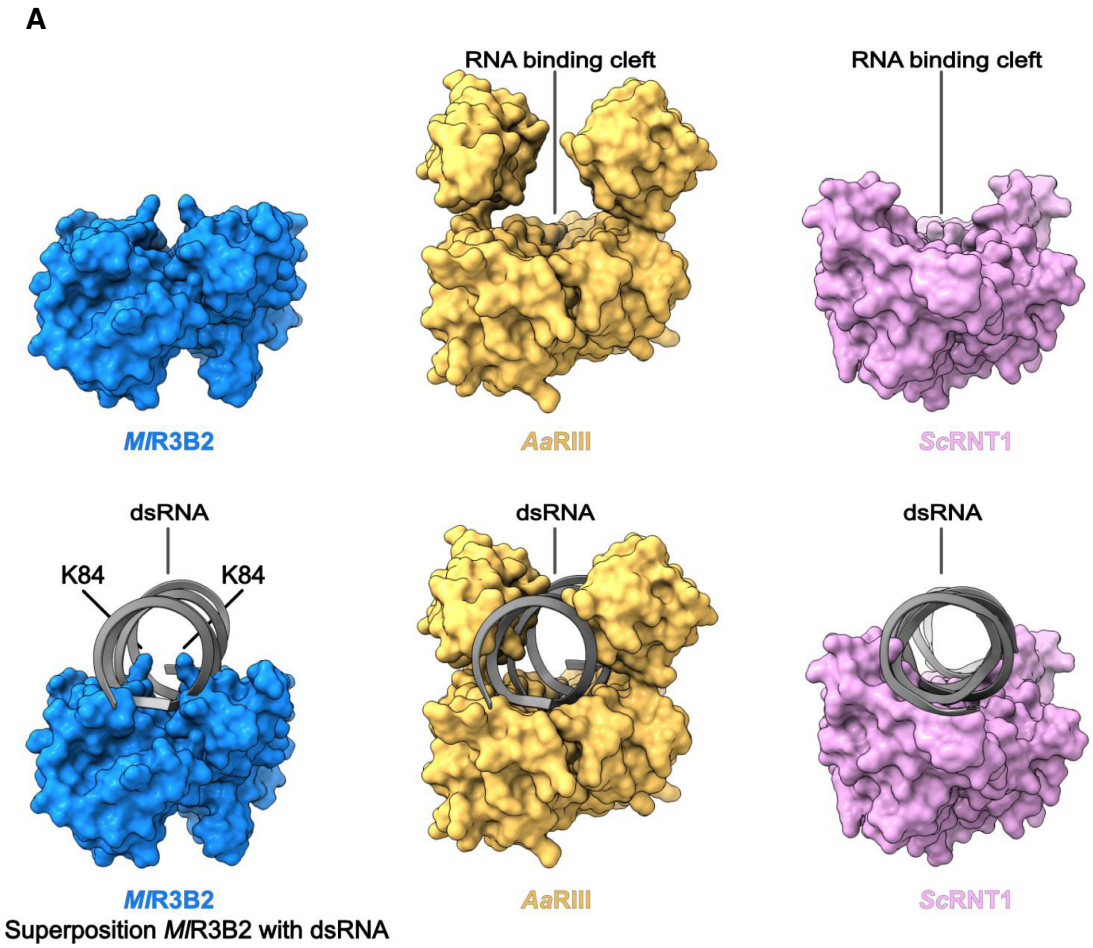

Figure 5. Analysis of RNA binding to the RNase III domain and *in vitro* activity of R3B2 K84 mutants. (**A**) Surface view of R3B2 and comparison with *Aa*RIII (PDB: 2NUG) and *Sc*RNT1 (PDB: 5T16)**.** For simplification, the dsRBD domains of *Sc*RNT1 are not shown**.** Top, structure of the indicated proteins without RNA. Bottom, structure of *Aa*RIII and *Sc*RNT1 bound to their dsRNA substrate and the dsRNA is modeled onto R3B2. (**B**) RNase activity assay performed as described in Figure 3 using wild-type R3B2 and the mutants in the catalytic center of the protein (20 nM *carB* ssRNA; 10 nM carB dsRNA; protein concentration: 150 nM). -, untreated.

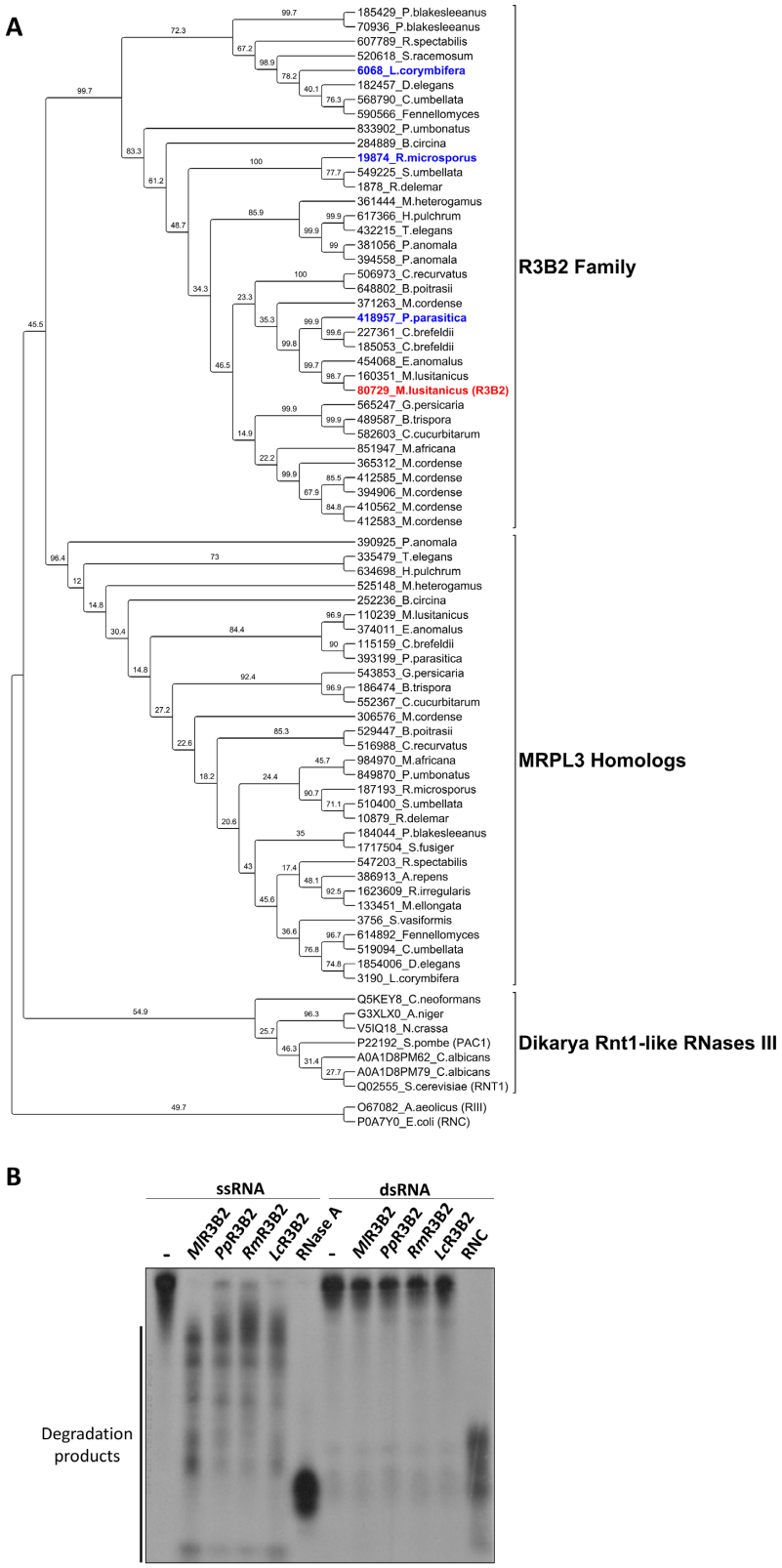

Figure 6. Phylogenetic and activity conservation in R3B2 family. (**A**) Maximum likelihood of amino acid sequences was analyzed with the LG +G+I+F (with four distinct gamma categories) phylogenetic model, which showed the lowest AIC value. The tree was rooted with class I RNase III sequences from bacteria (*A. aeolicus* and *E. coli*). The *M. lusitanicus* R3B2 was colored in red and the other R3B2 whose RNase activity was tested in blue. The numbers at branches correspond to bootstrap values generated with 1000 bootstrap replicates. A list with the JGI genome identifiers can be found in Supplementary Table S4. (**B**) *In vitro* RNase activity against of ssRNA and dsRNA of *M. lusitanicus* (*Ml*R3B2), *P. parasitica* (*Pp*R3B2), *R. microsporus* (*Rm*R3B2) and *L. corymbifera* (*Lc*R3B29) (20 nM *carB* ssRNA; 10 nM *carB* dsRNA; protein concentration: 300 nM). -, untreated.

and then selectively cleaves adjacent ssRNA regions was based on the essential role of RdRPs in NCRIP (19). Here, we have shown that R3B2, like typical class I RNases III (11,38), not only forms homodimers that are able to bind to dsRNA *in vitro*, but also to ssRNA. The RNA binding is sequence-independent *in vitro*, but depends on the presence of the two R3B2 dsRBDs given that the complete deletion of both dsRBDs abolished dsRNA binding. In particular, dsRBD2 appears to play a fundamental role because its mutation or deletion severely affected dsRNA-R3B2 complex stability. Although R3B2 can bind both dsRNA and ssRNA *in vitro*, it only shows degradation activity toward ssRNA substrates, whereas R3B2 is inert to completely dsRNA molecules. Interestingly, the degradation products observed *in vitro* reflect the degradation products of NCRIP observed *in vivo* (19). Loss of the ability to cut dsRNA depends only on the alterations in RIIID because a chimera, in which the R3B2 RIIID domain is replaced with the RNase III domain *E. coli* RNC (class I), degraded completely dsRNA molecules. This result clearly demonstrates that the unusual R3B2 substrate specificity is dictated by the structure of its atypical RIIID.

To obtain mechanistic insights into R3B2's atypical RIIID and its substrate preference for ssRNA, we determined the structure of a well-structured subtilisin-resistant fragment of R3B2 that included RIIID and the first dsRBD (dsRBD1), as the full-length protein was unstable. The structure of RIIID was well resolved, but density corresponding to dsRBD1 could not be observed, indicating that dsRBD1 is flexibly attached to the RIIID in the absence of an RNA substrate (38). Despite R3B2 sharing low sequence homology with typical RNases III, the overall structure of its RIIID superposed well with known RNase III structures. However, the structure revealed significant differences in the dsRNA binding motifs RBM3 and RBM4, which interact with the phosphoribose backbone of the dsRNA (38). In particular, RBM4 has been considerably reduced in length to only three amino acids and, therefore, interaction with RNA can be expected to be affected. This feature of a short RBM4 is conserved throughout R3B2-like proteins in other Mucorales. Positions of the acidic cluster in the R3B2 RIIID catalytic center was conserved, except for the presence of asparagine (N52) instead of an acidic residue. The presence of this residue could affect the affinity for magnesium ions and consequently, the RNA cleavage, but replacement of N52 with an acidic residue did not change the R3B2 cleavage specificity as no activity toward dsRNA observed. Interestingly, the two protomers of R3B2 form a tighter cleft compared to *Aa*RIII and *Sc*RNT, two typical class I RNases III (38,49), that would be incompatible with dsRNA binding. In particular, two lysine residues in R3B2 (K84) from the RIIID point toward the site that is used in *Aa*RIII and *Sc*RNT1 for dsRNA binding. Despite the presence of a positively charged amino acid in this position that is conserved throughout R3B2-like proteins from other Mucorales, its replacement by alanine, glutamate or glutamine to modify RNA-binding surface, or change the local charge or remove it respectively, did neither restore the dsRNA cleavage nor affect RNase activity against ssRNA. Therefore, it is tempting to speculate that the tight cleft could restrict the entry of the RNA substrate to the active site so that only ssRNA can reach the catalytic center of the R3B2 RIIID. Neither R3B2 nor NCRIP are likely to be a species-specific invention during the evolution of *M. lusitanicus* because R3B2 is conserved in Mucorales (19). Sequence similarity among R3B2 orthologs is low, and even includes amino acids in the RIIID catalytic domain, which are different among species and in any case correspond to the conserved amino acid in a canonical RIIID. Despite the differences from *Ml*R3B2, R3B2-like proteins from three evolutionary distant pathogenic Mucorales also showed activity only toward ssRNA *in vitro,* supporting the notion that the restriction for just ssRNA substrate is an inherent feature of its RIIID structure. These data suggest that the ancestor of Mucorales harbored as well an NCRIP mechanism to control gene expression at the post-transcriptional level that included an RdRP and a class I RNase III, wherein the RNase III evolved to lose the ability to cut dsRNA and conserved ssRNA cleavage competence. This transition allows NCRIP to regulate gene expression by degrading specific mRNA in sexual interaction and response to stress situations, such as phagocytosis by macrophages during the infection process (16,19). The evolutionary history of NCRIP and its mechanism of action remains an intriguing area of future study that may shed light on the evolution RNase III. Understanding how NCRIP responds to environmental challenges and select specific mRNAs for degradation may allow to progress in this unique regulatory mechanism.

DATA AVAILABILITY

The coordinates and the structure factors have been deposited in the Protein Data Bank with accession code PDB ID 6ZDW.

SUPPLEMENTARY DATA

Supplementary Data are available at NAR Online.

ACKNOWLEDGEMENTS

S.F. acknowledges E. Conti (MPI of Biochemistry) for continuous support

FUNDING

Ministerio de Economía y Competitividad, Spain [BFU2015-65501-P, co-financed by FEDER, and RYC-2014-15844]; Agencia Estatal de Investigación (AEI), Spain [PGC2018-097452-B-I00, co-financed by FEDER]; Ministerio de Educación, Cultura y Deporte, Spain [FPU16/01829 to J.T.C.-M.]; Agencia Estatal de Investigación (AEI)-Spain [PGC2018-094635-B-C22 to S.P.]; Ministerio de Economía y Competitividad, Spain [BIO2013-45336-R, co-financed by FEDER] and Fundación Séneca- Agencia de Ciencia y Tecnología de la Región de Murcia [19893/GERM/15, Programa de Apoyo a la Investigación 2014] to R.Z.-P. and Á.S.-F. Funding for open access charge: Agencia Estatal de Investigación, Spain [PGC2018-097452-B-I00, co-financed by FEDER].
Conflict of interest statement. None declared.

REFERENCES

1. Rabani,M., Levin,J.Z., Fan,L., Adiconis,X., Raychowdhury,R., Garber,M., Gnirke,A., Nusbaum,C., Hacohen,N., Friedman,N. *et al.* (2011) Metabolic labeling of RNA uncovers principles of RNA production and degradation dynamics in mammalian cells. *Nat. Biotechnol.*, **29**, 436–442.
2. Romero-Santacreu,L., Moreno,J., Pérez-Ortín,J.E. and Alepuz,P. (2009) Specific and global regulation of mRNA stability during osmotic stress in Saccharomyces cerevisiae. *RNA*, **15**, 1110–1120.
3. Cereghino,G.P. and Scheffler,I.E. (1996) Genetic analysis of glucose regulation in Saccharomyces cerevisiae: control of transcription versus mRNA turnover. *EMBO J.*, **15**, 363–374.
4. Liang,Y.-H., Costantino,N., Tropea,J.E., Shaw,G.X., Ji,X., Waugh,D.S., Court,D.L. and Gan,J. (2013) RNase III: genetics and function; structure and mechanism. *Annu. Rev. Genet.*, **47**, 405–431.
5. Gagnon,J., Lavoie,M., Catala,M., Malenfant,F. and Elela,S.A. (2015) Transcriptome wide annotation of eukaryotic RNase III reactivity and degradation signals. *PLoS Genet.*, **11**, e1005000.
6. Stead,M.B., Marshburn,S., Mohanty,B.K., Mitra,J., Castillo,L.P., Ray,D., Van Bakel,H., Hughes,T.R. and Kushner,S.R. (2011) Analysis of Escherichia coli RNase e and RNase III activity in vivo using tiling microarrays. *Nucleic Acids Res.*, **39**, 3188–3203.
7. Gitelman,D.R. and Apirion,D. (1980) The synthesis of some proteins is affected in RNA processing mutants of Escherichia coli. *Top. Catal.*, **96**, 1063–1070.
8. Carthew,R.W. and Sontheimer,E.J. (2009) Origins and mechanisms of miRNAs and siRNAs. *Cell*, **136**, 642–655.
9. Kwon,S.C., Nguyen,T.A., Choi,Y.G., Jo,M.H., Hohng,S., Kim,V.N. and Woo,J.S. (2016) Structure of human DROSHA. *Cell*, **164**, 81–90.
10. Liu,Z., Wang,J., Cheng,H., Ke,X., Sun,L., Zhang,Q.C. and Wang,H.W. (2018) Cryo-EM structure of human Dicer and its complexes with a pre-miRNA substrate. *Cell*, **173**, 1191–1203.
11. Liang,Y.H., Lavoie,M., Comeau,M.A., Elela,S.A. and Ji,X. (2014) Structure of a eukaryotic RNase III postcleavage complex reveals a double-ruler mechanism for substrate selection. *Mol. Cell*, **54**, 431–444.
12. Weinberg,D.E., Nakanishi,K., Patel,D.J. and Bartel,D.P. (2011) The inside-out mechanism of dicers from budding yeasts. *Cell*, **146**, 262–276.
13. Torres-Martínez,S. and Ruiz-Vázquez,R.M. (2017) The RNAi universe in fungi: a varied landscape of small RNAs and biological functions. *Annu. Rev. Microbiol.*, **71**, 371–391.
14. Binder,U., Maurer,E. and Lass-Flörl,C. (2014) Mucormycosis - from the pathogens to the disease. *Clin. Microbiol. Infect.*, **20**, 60–66.
15. Lax,C., Pérez-arques,C., Navarro-mendoza,M.I., Cánovas-márquez,J.T., Tahiri,G., Pérez-ruiz,J.A., Osorio-concepción,M., Murcia-flores,L., Navarro,E., Garre,V. *et al.* (2020) Genes, pathways, and mechanisms involved in the virulence of mucorales. *Genes (Basel).*, **11**, 317.
16. Pérez-Arques,C., Navarro-Mendoza,M.I., Murcia,L., Navarro,E., Garre,V. and Nicolás,F.E. (2020) A non-canonical RNAi pathway controls virulence and genome stability in Mucorales. *PLos Genet.*, **16**, e1008611.
17. Nicolás,F.E., Vila,A., Moxon,S., Cascales,M.D., Torres-Martínez,S., Ruiz-Vázquez,R.M. and Garre,V. (2015) The RNAi machinery controls distinct responses to environmental signals in the basal fungus Mucor circinelloides. *BMC Genomics*, **16**, 237.
18. Nicolas,F.E., Moxon,S., de Haro,J.P., Calo,S., Grigoriev,I. V, Torres-Martínez,S., Moulton,V., Ruiz-Vázquez,R.M. and Dalmay,T. (2010) Endogenous short RNAs generated by Dicer 2 and RNA-dependent RNA polymerase 1 regulate mRNAs in the basal fungus Mucor circinelloides. *Nucleic Acids Res.*, **38**, 5535–5541.
19. Trieu,T.A., Calo,S., Nicolás,F.E., Vila,A., Moxon,S., Dalmay,T., Torres-Martínez,S., Garre,V. and Ruiz-Vázquez,R.M. (2015) A non-canonical RNA silencing pathway promotes mRNA degradation in basal fungi. *PLos Genet.*, **11**, e1005168.
20. Calo,S., Nicolás,F.E., Lee,S.C., Vila,A., Cervantes,M., Torres-Martinez,S., Ruiz-Vazquez,R.M., Cardenas,M.E. and Heitman,J. (2017) A non-canonical RNA degradation pathway suppresses RNAi-dependent epimutations in the human fungal pathogen Mucor circinelloides. *PLos Genet.*, **13**, e1006686.
21. Calo,S., Shertz-Wall,C., Lee,S.C., Bastidas,R.J., Nicolás,F.E., Granek,J.A., Mieczkowski,P., Torres-Martínez,S., Ruiz-Vázquez,R.M., Cardenas,M.E. *et al.* (2014) Antifungal drug resistance evoked via RNAi-dependent epimutations. *Nature*, **513**, 555–558.
22. Chang,Z., Billmyre,R.B., Lee,S.C. and Heitman,J. (2019) Broad antifungal resistance mediated by RNAi-dependent epimutation in the basal human fungal pathogen Mucor circinelloides. *PLos Genet.*, **15**, e1007957.
23. Nicholson,A.W. (2014) Ribonuclease III mechanisms of double-stranded RNA cleavage. *Wiley Interdiscip. Rev. RNA*, **5**, 31–48.
24. Roncero,M.I.G. (1984) Enrichment method for the isolation of auxotrophic mutants of Mucor using the polyene antibiotic N-glycosyl-polifungin. *Carlsberg Res. Commun.*, **49**, 685–690.
25. James,P., Halladay,J. and Craig,E.A. (1996) Genomic libraries and a host strain designed for highly efficient two-hybrid selecton in yeast. *Genetics*, **144**, 1425–1436.
26. Nicolás,F.E., de Haro,J.P., Torres-Martínez,S. and Ruiz-Vázquez,R.M. (2007) Mutants defective in a Mucor circinelloides dicer-like gene are not compromised in siRNA silencing but display developmental defects. *Fungal Genet. Biol.*, **44**, 504–516.
27. Gietz,R.D., Schiestl,R.H., Willems,A.R. and Woods,R.A. (1995) Studies on the transformation of intact yeast cells by the LiAc/SS-DNA/PEG procedure. *Yeast*, **11**, 355–360.
28. Lorenz,R., Bernhart,S.H., Höner zu Siederdissen,C., Tafer,H., Flamm,C., Stadler,P.F. and Hofacker,I.L. (2011) ViennaRNA Package 2.0. *Algorithms Mol. Biol.*, **6**, 26.
29. Winter,G., Lobley,C.M.C. and Prince,S.M. (2013) Decision making in xia2. *Acta Crystallogr. D. Biol. Crystallogr.*, **69**, 1260–1273.
30. Winn,M.D., Ballard,C.C., Cowtan,K.D., Dodson,E.J., Emsley,P., Evans,P.R., Keegan,R.M., Krissinel,E.B., Leslie,A.G.W., McCoy,A. *et al.* (2011) Overview of the CCP4 suite and current developments. *Acta Crystallogr. D. Biol. Crystallogr.*, **67**, 235–242.
31. Terwilliger,T.C., Adams,P.D., Read,R.J., McCoy,A.J., Moriarty,N.W., Grosse-Kunstleve,R.W., Afonine,P. V, Zwart,P.H. and Hung,L.W. (2009) Decision-making in structure solution using Bayesian estimates of map quality: the PHENIX AutoSol wizard. *Acta Crystallogr. D. Biol. Crystallogr.*, **65**, 582–601.
32. Emsley,P., Lohkamp,B., Scott,W.G. and Cowtan,K. (2010) Features and development of Coot. *Acta Crystallogr. D. Biol. Crystallogr.*, **66**, 486–501.
33. Murshudov,G.N., Vagin,A.A. and Dodson,E.J. (1997) Refinement of macromolecular structures by the maximum-likelihood method. *Acta Crystallogr. D. Biol. Crystallogr.*, **53**, 240–255.
34. Afonine,P. V, Grosse-Kunstleve,R.W., Echols,N., Headd,J.J., Moriarty,N.W., Mustyakimov,M., Terwilliger,T.C., Urzhumtsev,A., Zwart,P.H. and Adams,P.D. (2012) Towards automated crystallographic structure refinement with phenix.refine. *Acta Crystallogr. D. Biol. Crystallogr.*, **68**, 352–367.
35. Goddard,T.D., Huang,C.C., Meng,E.C., Pettersen,E.F., Couch,G.S., Morris,J.H. and Ferrin,T.E. (2018) UCSF ChimeraX: meeting modern challenges in visualization and analysis. *Protein Sci.*, **27**, 14–25.
36. Edgar,R.C. (2004) MUSCLE: a multiple sequence alignment method with reduced time and space complexity. *BMC Bioinformatics*, **5**, 113.
37. Guindon,S., Dufayard,J.F., Lefort,V., Anisimova,M., Hordijk,W. and Gascuel,O. (2010) New algorithms and methods to estimate maximum-likelihood phylogenies: assessing the performance of PhyML 3.0. *Syst. Biol.*, **59**, 307–321.
38. Gan,J., Tropea,J.E., Austin,B.P., Court,D.L., Waugh,D.S. and Ji,X. (2006) Structural insight into the mechanism of double-stranded RNA processing by ribonuclease III. *Cell*, **124**, 355–366.
39. Carey,J. (2000) [30]A systematic and general proteolytic method for defining structural and functional domains of proteins. *Methods Enzymol.*, **328**, 499–514.
40. Ji,X. (2008) The mechanism of RNase III action: how dicer dices. *Curr. Top. Microbiol. Immunol.*, **320**, 99–116.
41. Hellman,L.M. and Fried,M.G. (2007) Electrophoretic mobility shift assay (EMSA) for detecting protein-nucleic acid interactions. *Nat. Protoc.*, **2**, 1849–1861.
42. Masliah,G., Barraud,P. and Allain,F.H.T. (2013) RNA recognition by double-stranded RNA binding domains: a matter of shape and sequence. *Cell. Mol. Life Sci.*, **70**, 1875–1895.
43. Sun,W., Jun,E. and Nicholson,A.W. (2001) Intrinsic double-stranded-RNA processing activity of Escherichia coli

ribonuclease III lacking the dsRNA-binding domain. *Biochemistry*, **40**, 14976–14984.
44. Redko,Y., Bechhofer,D.H. and Condon,C. (2008) Mini-III, an unusual member of the RNase III family of enzymes, catalyses 23S ribosomal RNA maturation in B. subtilis. *Mol. Microbiol.*, **68**, 1096–1106.
45. Robertson,H.D., Webster,R.E. and Zinder,N.D. (1968) Purification and properties of ribonuclease III from Escherichia coli. *J. Biol. Chem.*, **243**, 82–91.
46. Dunn,J.J. (1976) RNase III cleavage of single stranded RNA. Effect of ionic strength on the fidelity of cleavage. *J. Biol. Chem.*, **251**, 3807–3814.
47. Li,H. lin, Chelladurai,B.S., Zhang,K. and Nicholson,A.W. (1993) Ribonuclease III cleavage of a bacteriophage T7 processing signal. Divalent cation specificity, and specific anion effects. *Nucleic Acids Res.*, **21**, 1919–1925.
48. Gan,J., Shaw,G., Tropea,J.E., Waugh,D.S., Court,D.L. and Ji,X. (2008) A stepwise model for double-stranded RNA processing by ribonuclease III. *Mol. Microbiol.*, **67**, 143–154.
49. Song,H., Fang,X., Jin,L., Shaw,G.X., Wang,Y.X. and Ji,X. (2017) The functional cycle of Rnt1p: five consecutive steps of double-stranded RNA processing by a eukaryotic RNase III. *Structure*, **25**, 353–363.
50. Partin,A.C., Zhang,K., Jeong,B.C., Herrell,E., Li,S., Chiu,W. and Nam,Y. (2020) Cryo-EM structures of human Drosha and DGCR8 in complex with primary microRNA. *Mol. Cell*, **78**, 411–422.
51. MacRae,I.J., Zhou,K., Li,F., Repic,A., Brooks,A.N., Cande,W.Z., Adams,P.D. and Doudna,J.A. (2006) Structural basis for double-stranded RNA processing by Dicer. *Science*, **311**, 195–198.
52. Grigoriev,I. V., Nikitin,R., Haridas,S., Kuo,A., Ohm,R., Otillar,R., Riley,R., Salamov,A., Zhao,X., Korzeniewski,F. *et al.* (2014) MycoCosm portal: gearing up for 1000 fungal genomes. *Nucleic Acids Res.*, **42**, D699–D704.
53. Walther,G., Wagner,L. and Kurzai,O. (2019) Outbreaks of Mucorales and the species involved. *Mycopathologia*, **185**, 765–781.
54. Hassan,M.I.A. and Voigt,K. (2019) Pathogenicity patterns of mucormycosis: epidemiology, interaction with immune cells and virulence factors. *Med. Mycol.*, **57**, S245–S256.
55. Cerutti,H. and Casas-Mollano,J.A. (2006) On the origin and functions of RNA-mediated silencing: from protists to man. *Curr. Genet.*, **50**, 81–99.
56. Aguado,L.C. and TenOever,B.R. (2018) RNase III nucleases and the evolution of antiviral systems. *Bioessays*, **40**, 1700173.